DOI:
10.1088/1741-2552/ac7c8f

Document Version
Peer reviewed version

Chronic recording of the vagus nerve to analyze modulations by the light-dark cycle

Hugo Smets[1], *Lars Stumpp*[2], *Javier Chavez*[1], *Joaquin Cury*[1], *Louis Vande Perre*[1], *Pascal Doguet*[3], *Anne Vanhoestenberghe*[4], *Jean Delbeke*[2], *Riëm El Tahry*[2], *Antoine Nonclercq*[1]

[1] Bio, Electro and Mechanical Systems (BEAMS), Université Libre de Bruxelles, Brussels, Belgium
[2] Institute of Neurosciences (IONS), Université Catholique de Louvain, Brussels, Belgium - Cliniques Universitaires Saint Luc, Department of Neurology, Brussels, Belgium
[3] Synergia Medical SA, Mont-Saint-Guibert, Belgium
[4] Implanted Devices Group, University College London, London, U.K.

E-mail: hugo.smets@ulb.be

Abstract

Objective. The vagus nerve is considered to play a key role in the circadian rhythm. Chronic continuous analysis of the vagus nerve activity could contribute to a better understanding of the role of the vagus nerve in light-dark modulations. This paper presents a continuous analysis of spontaneous vagus nerve activity performed in four rats. **Approach.** We analyzed the vagus electroneurogram (VENG) and electroencephalogram (EEG) over a recording period of 28 days. Spike activity and heart rate estimation were derived from the VENG, and slow-wave activity was derived from the EEG. The presence of repetitive patterns was investigated with periodograms, cosinor fitting, autocorrelation, and statistical tests. The light-dark variations derived from the VENG spikes were compared with EEG slow waves, an established metric in circadian studies. **Results.** Our results demonstrate that light-dark variations can be detected in long-term vagus nerve activity monitoring. A recording period of about seven days is required to characterize accurately the VENG light-dark variations. **Significance.** As a major outcome of this study, vagus nerve recordings hold the promise to help understand circadian regulation.

Keywords: chronic recording, vagus nerve activity, circadian rhythm, light-dark modulations, epilepsy.

1. INTRODUCTION

The circadian rhythm is a natural, internal process, characterized by a 24-hour self-sustained pattern. It has been widely studied and yet is only partially understood. It is well known that the central and peripheral autonomic nervous systems have an important role in distributing the circadian signals from the hypothalamic suprachiasmatic nucleus (SCN) clock. This control on the peripheral organs [1], [2] is reflected by 24-hour variations in melatonin, cortisol, and body temperature, for example. In addition, various non-SCN brain regions (e.g. hypothalamic nuclei, forebrain, olfactory bulb, and pineal gland) and non-neuronal tissues (e.g. liver, kidney, muscle, adipose tissue, and blood cells) contain autonomous oscillators [3]. Central and peripheral clocks communicate, probably through hormonal cascades, metabolites, or other circulating factors, but exact mechanisms are still not fully understood.

The circadian rhythm can be monitored through many physiological markers. For example, Makino *et al.* [4] and Oosting *et al.* [5] demonstrated the circadian rhythm of blood pressure (BP), heart rate (HR), and the role of the autonomic nervous system. Hu *et al.* [6] also describe a circadian rhythm of HR

driven by the SCN. The impact of the circadian rhythm on sympathetic activity, cardiac vagal modulation, cortisol, and other parameters has been explored [7].

The vagus nerve is considered to have a key role in the circadian rhythm. An increase in vagal tone at night is believed to be linked to the SCN clock [8]. Bando *et al.* [9] have shown in rats, through vagotomy, that SCN regulation signals are transmitted by the vagus nerve. In one study performed in dogs, simultaneous monitoring of left stellate ganglion nerve activity, vagal nerve activity, and electrocardiography was obtained before and after pacing-induced congestive heart failure [10]. Surprisingly, results showed a circadian rhythm in the activity recorded from the left stellate ganglion nerve, but the same observation did not reach statistical significance in the thoracic portion of the left vagus nerve, although a circadian rhythm seems to be visible on the reported vagus nerve activity.

While the role of the autonomic nervous system on circadian regulation has been widely investigated, literature on the manifestation of the circadian rhythm in peripheral neural activity is scarcer. More specifically, to the best of our knowledge, except for one paper [11], no continuous long-term analysis of vagus nerve regulatory effect in the context of the circadian rhythm has been published to this day. Recently, the chronic recording of the vagus nerve has been developed and several studies reported the feasibility of such recordings [12]–[15]. Chronic continuous analysis of the vagus nerve activity could contribute to the understanding of the role of the vagus nerve in the circadian oscillations in general, and could be of special interest in the frame of epilepsy [16], [17]. In this paper, we present for the first time the 24-hour patterns of spontaneous vagus nerve activity found in continuous chronic vagus nerve recordings performed in four rats, which was previously reported only by indirect measurement. In this regard, this methodological article is a proof of feasibility to allow further studies of the mechanisms underlying circadian modulation through chronic direct vagus nerve measurement in rats.

2. METHODS

2.1. SURGICAL PROCEDURE

Four male Wistar rats (3 – 5 months, 350 – 420 g) obtained from the local animal facility were used. All rats were provided with ad libitum access to food and water under a 12-hour light-dark cycle. The experimental procedure has been approved by the University Health Sciences Sector Laboratory Animal Protection Committee (2018/UCL/MD/001). The animals were injected with 100 mg/kg Ketamine and 7 mg/kg Xylazine intraperitoneally. The level of anesthesia was controlled by the withdrawal reflex upon noxious paw stimulation and maintained by additional intraperitoneal injections of 60 mg/kg Ketamine, approximately every 30 minutes. The body temperature was controlled via a rectal probe and maintained at 37.5°C by a heating pad. Buprenorphine was administered (0.05 mg/kg) for its analgesic effects before and after the surgery.

All animals were implanted with homemade epidural electroencephalogram (EEG) electrodes using watchmaker screws (Plastics1, Roanoke, VA, USA), and a micro-cuff electrode around the left cervical vagus nerve for vagus electroneurogram (VENG) recording (Microprobes for Life Science, Gaithersburg, MD, USA). The cuff is 10 mm long, has an inner diameter of 300 µm, and contains three ring electrodes made of 50 µm Pt/Ir strips spaced by 4 mm. The vagus nerve was exposed (but not desheated for the nerve viability) and the cuff was placed around the nerve (see Figure 1b), closed with sutures (embedded in the cuff), and surgical adhesive (KwikSil, World Precision Instruments, Sarasota, FL, USA) was applied to close the cuff. An additional layer of implantable silicone (MED4-4220, NuSil Technology, Carpinteria, CA, USA) was added to cover the leads to prevent them from breaking around

the head connector area. Epidural electrodes were implanted by screwing in the previously drilled holes (described in Figure 1a) as the rat was placed in a stereotactic frame (David Kopf Instruments, Tujunga, CA, USA). One of these is used as a VENG reference. The 8 electrodes (5 epidural electrodes and 3 ring electrodes in the cuff) were assembled in a head stage connector placed on the rat skull and fixed with dental cement. The head stage connector is 3D-printed to fit a 2-row-4-way 2.54-mm connector, and is secured by a custom-made clamp.

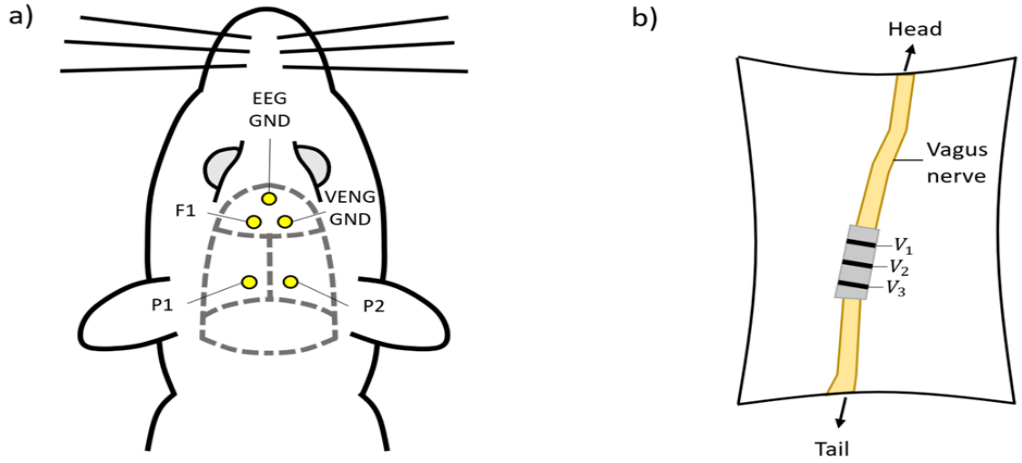

Figure 1. a) Position of the epidural electrodes, with spatial values relative to the bregma. EEG ground (5 mm anterior, 0 mm lateral), VENG ground (2 mm anterior, 3 mm lateral (right)), EEG frontal 1 (2 mm anterior, 3 mm lateral (left), F1 in the drawing) and the two parietal EEG contacts (5 mm posterior, 3 mm lateral (left and right), P1 and P2 in the drawing). Two EEG bipolar channels are recorded: P1-F1 and P2-F1 (i.e., F1 is used as a common electrode for both EEG bipolar inputs). b) Schematic description of the cuff electrodes. V_1 *-* V_2 *are used as the bipolar inputs of one VENG channel, and* V_3 *-* V_2 *are used as the bipolar inputs of the other VENG channel. The two channels can be added to obtain a true tripolar configuration or subtracted to obtain a bipolar configuration. We used it as bipolar to ensure a large interelectrode distance* [18], [19].

2.2. DATA ACQUISITION

One VENG channel with bipolar/tripolar recording capabilities and two bipolar EEG channels were used. Both VENG and EEG channels had an isolated ground placed on the forehead of the rat (respectively, VENG GND and EEG GND, see Figure 1a). We used the VENG bipolar configuration as the input signal to ensure a large interelectrode distance [18], [19]. We used P1-F1 derivation as the EEG input signal.

For the VENG channels, pre-amplifiers were placed as close as possible to the rat (i.e. near the slip ring that allows the rat to move freely [20]) to minimize noise, movement artifacts and capacitive interferences. Although important for the low amplitude neural signals [21], [22], this precaution was not necessary for the much larger EEG signals, similarly to previously proposed chronic recording setups [20].

The three contacts of the cuff electrodes feed two amplification channels which are digitized separately to be later combined by software. The custom-made amplifiers were previously designed and validated [23]. Hardware filters with a passband 12 to 10,000 Hz for VENG and 0.16 to 80 Hz for EEG were used (1st order passive HP filters and 4th order active LP filter). The gain of the amplifier is 800 and the observed amplifier root mean square noise is 0.5 µV referred to the input in the spectrum of the VENG and 0.3 µV in the spectrum of the EEG. The VENG and EEG signals were acquired respectively at 40 kHz and 250 Hz via a USB-6212 multifunction I/O-device (National Instruments, Austin, USA) for an overall resolution of 0.175 µV per bit and an input dynamic range of ±3.5 mV. The software filters consist of a 2nd order Butterworth passband from 300 Hz to 3000 Hz for the VENG and from 2 Hz to 35 Hz for the EEG. A custom-made MATLAB R2017a application (MathWorks, Natick, USA)

was used to acquire the data. The VENG and EEG were recorded in a bipolar differential mode. A video was acquired with a night-vision camera module for Raspberry Pi, synchronized with a Raspberry Pi 4 (Raspberry Pi Limited, Cambridge, UK), linked to the signal recording MATLAB application.

2.3. CHRONIC RECORDING

The rats were placed in a quiet recording room. A recovery period of 10 to 14 days was observed after the surgery. Throughout the experiment, the animals were checked daily for signs of stress and otherwise left undisturbed, and the light-dark cycle was kept constant. The rats were provided with ad libitum access to food and water. Cages were cleaned once a week. During the recordings, the rats were connected by their head stage and free to move without feeling the weight of the cable as a balanced swing is used [20].

The electrode impedance was measured every week with an impedance meter at 1 kHz (Microprobes for Life Science, Gaithersburg, MD, USA).

Attention has been paid specifically to validate the VENG recordings:

(1) Right after the surgery, a recording was realized while the animal was still anesthetized, so without any movement artifacts, to assess the quality of the signal.
(2) During the chronic experiment, electrodes impedances were controlled.
(3) We used a previously validated spike detection algorithm [24] to quantify spike activity in the VENG signal acquired chronically. The shape of the spikes was also visually validated. For instance, only spikes with a length below 1.5 ms were considered valid.
(4) A post-mortem dissection was performed to confirm the contact between the electrodes and the nerve.

2.4. DATA PROCESSING

The flowchart to obtain the physiological parameters averaged on a 1-h basis can be visualized in Figure 2. It is further detailed in sections 2.4.1, 2.4.2, and 2.4.3.

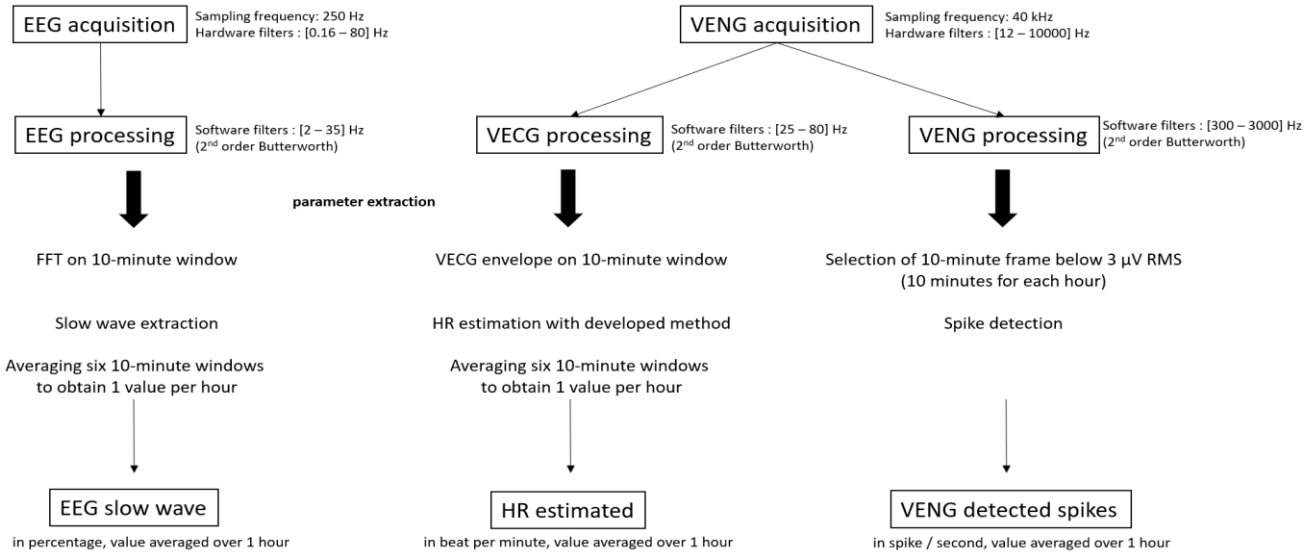

Figure 2 Flowchart of the data processing to extract the physiological parameters averaged on a 1-h basis.

2.4.1.EEG processing

The major tasks related to EEG data processing to compute slow waves are presented in Figure 2, left. The EEG was software filtered from 2 to 35 Hz (2nd order Butterworth). The frequency power spectrum was extracted by applying a fast Fourier transform on 10-minute frames of the 250-Hz sampled signal. The power of the slow-wave band (2 to 7 Hz) relative to the total spectrum of the filtered signal was then computed by taking the ratio of the two values. The result was used to characterize the state of the animal since slow waves (delta, theta) occur when the animal is asleep [25]. The slow-wave values were averaged over 1-hour periods.

2.4.2.VENG processing

The major tasks related to VENG data processing to detect spikes are presented in Figure 2, right. The VENG was software filtered between 300 and 3000 Hz (2nd order Butterworth). The number of spikes per second obtained for each hour of the recording was computed using a spike detection algorithm adapted from [17], [26]–[28]. Spike are detected based on their waveform (template matching), with templates that are automatically adapted to each subject (subject-specific templates) and based on specific features of the waveform (spike slope, curvature, and duration). The SNR, computed as the RMS value of the spikes divided by the RMS value of the corresponding 10-minute signal (expressed in dB), was used to evaluate the spike detection. To avoid motion artifacts, a 10-minute sample with a signal below 3 µV RMS in 20-second averages was extracted from each hour of recording. Then, the number of spikes detected in these 10 first minutes showing no motion artifact (as defined above) was averaged and expressed in spikes per second (with one value per hour of recording). Consequently, the same data length (10 minutes) was picked up from each one hour recording section considered for further data processing.

2.4.3.HR processing

The major tasks related to VENG data processing to compute the HR estimate are presented in Figure 2, center. Preliminary experimentation on rats under ketamine anesthesia (8 recordings of 15 minutes) with simultaneous ECG recording showed that VENG signal filtered in a 25 to 80 Hz passband (2nd order Butterworth) has an envelope with peaks that tend to be synchronous with ECG QRS peaks. These recordings were realized acutely in chronically implanted rats under anesthesia, about one month after implantation. Figure 3a shows an example of a recording from a chronically implanted rat under anesthesia. The envelope peaks of the VENG can be compared to the ECG signal. Based on this observation, the VENG signal was filtered in a 25 to 80 Hz range (2nd order Butterworth). Then, the envelope-derived heart frequency, called VECG, was computed using the peak envelope (MATLAB *envelope* function), determined using spline interpolation over local maxima separated by at least 40 ms of samples. The VECG approaches globally the HR calculated from the ECG, but the variations on the signal (59 beats per minute (bpm) rms vs 4 bpm rms in the ECG) were considered too high to correctly estimate the beat-to-beat HR (see Figure 3b). In this study, for each hour of recording, VECG-based HR estimation was computed over 10-minute windows and then averaged over one-hour periods, such that one hour is averaged by 6 values of the corresponding 10-minute averaged HR. For each 10-minute frame, the VECG estimate of the average HR was obtained by taking the maximum of the VENG frequency distribution histogram (see Figure 3c). We chose to use this value, corresponding to the HR value the most represented in the window, as the reference HR value over 10 minutes (rather than using an instantaneous value). Taking the maxima of the histogram enhances the robustness of the estimation (as compared to taking the average of VENG-based HR estimations) because outliers automatically are rejected (see Figure 2c). In this example, the rat showed an average HR estimation of 427 bpm, as estimated by the VECG, while the HR was 432 bpm as measured from the ECG. In this paper, the HR data presented in the result section is the VECG-based HR derived as described here.

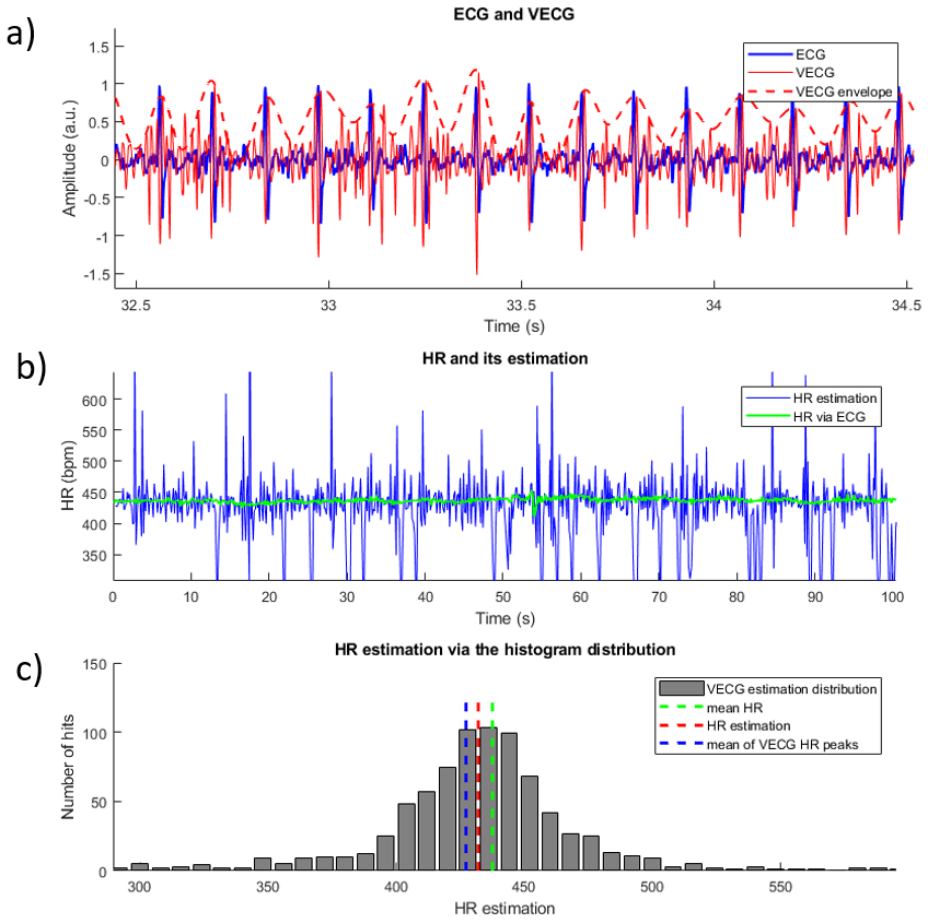

Figure 3. a) ECG (blue) and VENG (plain red line) filtered in a (25 – 80) Hz bandpass, and corresponding VENG envelope (red dashed lines). The VENG envelope and the ECG peak around the same rate. b) HR measured from ECG (green) and estimated with VECG (blue). The estimations follow globally the HR, but the SNR was considered too low to correctly estimate the beat-to-beat HR. c) Histogram of the VECG-based HR estimation. The maximum VECG histogram peak is taken as the estimated mean HR (red dashed lines). The mean of the VECG is shown in blue dashed lines (for comparison). The mean HR measured from ECG is shown in green dashed lines. The mean HR measured from ECG is better estimated by the maximum of the VECG distribution histogram than by mean VECG.

This method has been validated with a Bland-Altman plot (see Figure 4). The Bland-Altman plot was estimated on 8 sets of 15-minute recordings from an anesthetized rat with 60 mg/kg ketamine only. The agreement intervals were [-19, 28], [-16, 22], [-11, 13], and [-8, 14] for HR estimation over a period of 2, 4, 8 and 10 minutes respectively, and the mean error is kept below 5 bpm for all periods. The data is normally distributed (verified with Kolmogorov-Smirnov test, $p > 0.05$). A slight positive trend can be seen in Figure 4 (larger differences for larger means). Simple linear regression was used, and the fitted regression model was: difference = -31.3 + 0.077 * mean ($R^2 = 0.017$). This means that the method could slightly underestimate the HR variations (up to about 8%). As expected, estimation of HR over a larger period reduces the standard deviation of the errors, from 11.9 bpm to 5.6 bpm. A 10-minute window was considered sufficient for HR estimation.

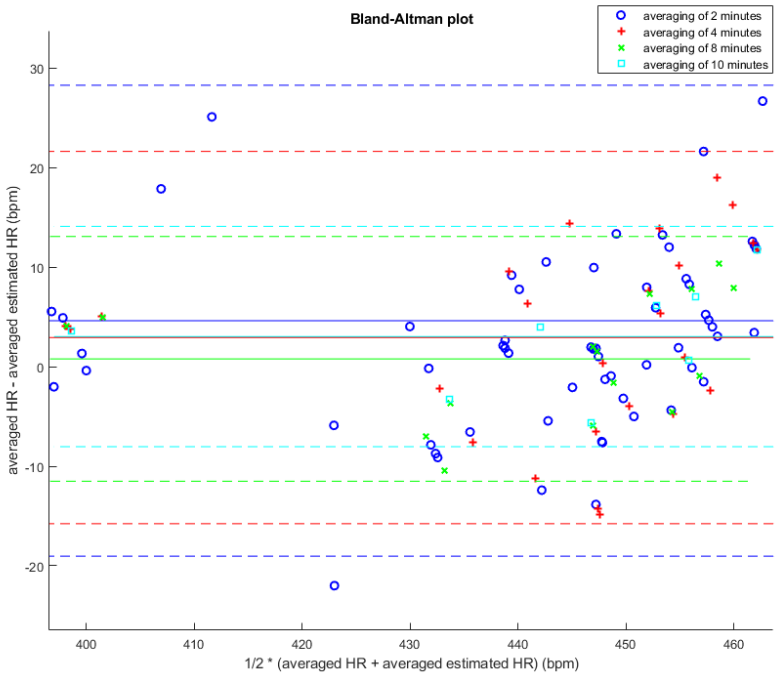

*Figure 4. Bland-Altman plot for the estimation of HR compared to the HR calculated with the ECG signal. The x-axis represents the mean of the averaged HR and the averaged estimated HR, and the y-axis represents the difference between the averaged values. In plain lines, the mean error of the estimation. In dashed lines, the agreement interval (i.e. 1.96 * std of the error). The mean error is kept below 5 bpm.*

The values obtained in the chronic recordings (see Results) were lower than the ones obtained in the ketamine-anesthetized rat, as expected because the effect of anesthesia with ketamine increases HR in rats, up to around 432 ± 11 bpm [29].

2.5. STATISTICAL TESTS

Statistical tests were performed to assess light-dark cycles, on EEG slow-wave activity, HR, and VENG spike activity. As mentioned in the previous section, all metrics used are averaged over 1-hour periods, thus yielding 24 points to describe 1 day of recording.

Periodograms have been used to detect repetitive patterns [30], a repetitive pattern corresponding to a peak in the periodogram. The periodogram was obtained with a Fourier analysis of the 1-hour averaged values of the physiological metrics over 5 or 10 days. The significance of the peak was evaluated with Fisher's g-statistic. If a peak is significant, it means that the duration associated to it is a non-random repetitive period.

The entire recordings were averaged by frames of two consecutive days. Therefore, for 28 days of recording, the 48-h data were averaged 14 times. The resulting 48-h averaging can be divided in two days, each of them having one dark period and one light period. After the normality check (Kolmogorov-Smirnov), one-way ANOVA was used to confirm the light-dark cycles of physiological signals (HR, EEG slow-wave and VENG spike activity), as previously proposed [30]–[32]. Statistical tests were applied to the results of the averaged 48-h frames. To check stability, the mean of the physiological signals was compared by one-way ANOVA (1) between 2 consecutive periods of 24 h, (2) between the first and the second light period, (3) between the first night and the second dark period. To check the light-dark cycles, (4) the first light period was compared by one-way ANOVA with and the first dark period.

The autocorrelation of the 48-hour averaged signal was calculated to confirm the 24-hour rhythmicity while showing a time lag. In autocorrelation, the correlations ranging inside the confidence interval are considered as random and not due to a periodic pattern; the correlations beyond the confidence interval are considered as exhibiting a repetitive pattern. The maxima of the autocorrelation (for lags > 0h) correspond to the period of the repeating pattern. The amplitude of the corresponding peaks represents the degree of similarity between the signal analyzed and a lagged version of itself, yielding an amplitude value of +1 for a perfect positive correlation.

The cosinor method was finally used to fit the data with a pre-defined 24-hour period. The probability of a non-zero amplitude of the oscillations was assessed based on the cosinor curve [33]. The cosinor method consists of fitting cosine curves with an *a priori* known period to estimate the smooth rhythm described by the circadian rhythm [30]. Cosinor analysis uses the least-squares method to fit a sine wave to a time series. The amplitude of oscillations and the curve phase are output parameters describing the variations. The existence of a non-zero amplitude [34] is assessed by testing the overall significance of the cosinor model with the residual sum of square by an F-ratio described as:

$$F = \frac{\frac{\sum\left(\hat{Y}_i - \bar{Y}\right)^2}{2}}{\frac{\sum(Y_i - \bar{Y})^2}{N-3}}$$

where N is the number of points, $\bar{Y}$ is the arithmetic mean of observed values, $\hat{Y}_i$ is the *i*th estimated value, and Y_i is the *i*th observed value. The zero-amplitude hypothesis is rejected when $F > F_{1-\alpha}(2, N-3)$, with $\alpha = 0.05$, therefore $F > 3.20$ in our case.

To calculate the number of days required to evaluate the light-dark cycles, the average over the entire recording length is compared with averages of n days, n varying from 2 to the maximum. The average is performed for each hour of the day individually, so for a given hour (hour h), the average is computed over n points (on each hour h of n days). The Pearson's correlation coefficient is obtained. A correlation above 0.8 is considered as being very strong [35]. Beyond this value, it is expected that the average will not change much, therefore the number of days to establish this average is sufficient.

3. RESULTS

3.1. GENERAL OUTCOME

Four rats were successfully implanted and recorded for 28 days. The electrode impedances were measured each week. In one rat (rat 3), the electrode leads broke (at the level of the head connector) three weeks after the beginning of the recording, as detected by high impedance measurements and confirmed in postmortem analysis.

Specific attention to VENG recordings (as stated in section 2.3), revelated the following:

(1) For all rats, visual inspection of the recording, realized while the animal was still anesthetized, showed that the signal was genuine and corresponded to previously validated VENG signal [17]. Respiration bursts were also consistently observed, which further confirmed its neural origin.
(2) During the chronic experiment, electrodes impedances remained stable (-13 % ± 18 % of their initial value, measured at 1kHz). The impedances equaled 2.1 kΩ, 4.4 kΩ, 6.0 kΩ, 5.4 kΩ at the

beginning of the recording, and 2.4 kΩ, 3.6 kΩ, 4.5 kΩ, 4.2 kΩ at the end of the recording, respectively for rat 1 to 4.

(3) The post-mortem dissection revealed that, for all the rats, the electrodes were still in contact with the nerve.

Signal processing and statistical analysis were performed on all rats, for 28 days in three rats (1, 2 and 4) and for 21 days in one rat (3).

Figure 5 shows the SNR of the spikes detected in the VENG on day 1, day 14, and day 28 of the recordings. The SNR was stable and sufficient to identify spikes (SNR > 5 dB) during the entire recording and for all rats.

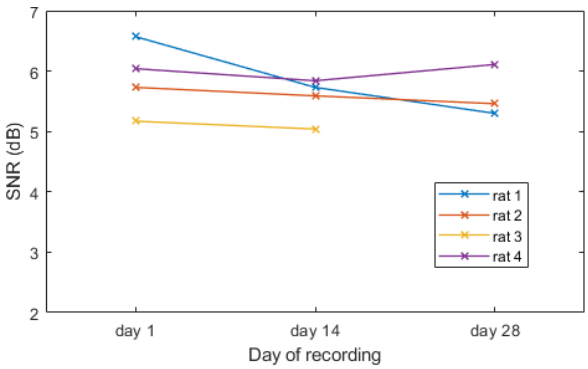

Figure 5. SNR of the spikes detected in the VENG over time.

The raw signal was visually analyzed to assess its validity as previously proposed [36]. The VENG baseline was 1.7 ± 0.6 µV RMS. The proportion of data that was rejected (i.e. above 3 µV RMS) was 23%, 9 %, 27%, 20%, respectively for rats 1 to 4. Figure 6 illustrates VENG and EEG examples for a 10-minute frame, in rat 1.

EEG data quality has been visually validated, both during awake and sleep phases. In awake phases, inspection included sections with and without rat motion. The motion artifacts did not contaminate much the EEG signal, in the 2-35 Hz bandwidth, so no specific artifact rejection data processing was used.

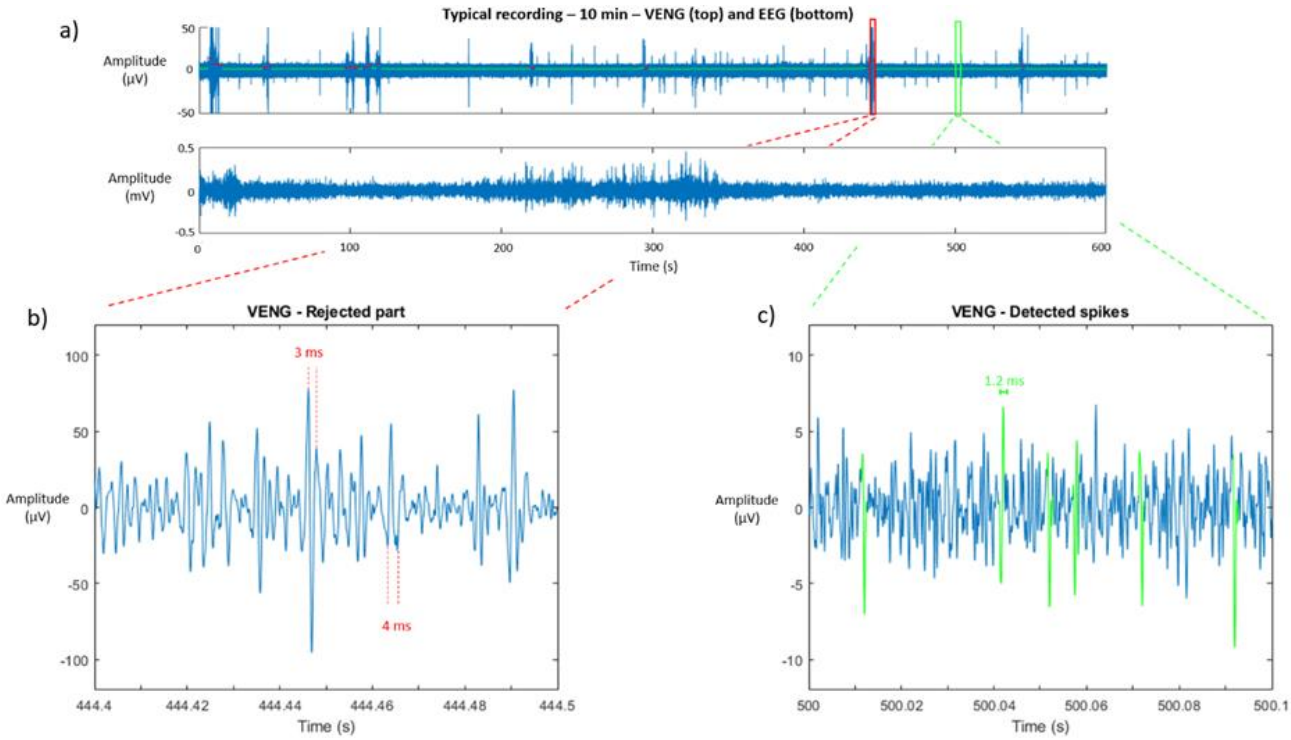

Figure 6. (a): 10 minutes of typical VENG recording of rat 1. (b) and (c): illustrations of rejected and detected spikes from the portion of signal corresponding, respectively, to the red and green box of (a). See Section 2.4.2. for the description of the spike detection algorithm. (b) is mainly composed of large amplitude artifacts, with relatively long durations (> 3 ms), probably originating from motion or muscular artifacts (described as longer than 2 ms in [12]*). (c) comprises spikes (in green) with shape and specific features within the range spike detection algorithm (see Section 2.4.2.). For instance, the duration of the detected spikes is shorter than 1.5 ms (in line with* [12]*).*

Figure 7 shows EEG slow-wave activity, HR, and the VENG spike activity during two-day timeframes averaged over the entire recording length.

A 24-hour pattern linked to the spikes detected in the VENG activity can be observed in all the rats, even if variations are seen between animals. During the dark period, we observe in two rats (2 and 3) an increase of the HR and, for all rats, an increase of the VENG spike activity. During the light period, we observe a decrease of the HR in two rats (2 and 3), and, for all rats, a decrease of the VENG spike activity, and an increase of the EEG slow-wave activity. The large peak of EEG slow-wave activity between 8 A.M. and 10 A.M. corresponds to sleep (delta and theta waves).

HR variations were visible for rats 2 and 3. There were no clear HR variations for rats 1 and 4, probably due to the limitations of our method (as detailed in the Discussion section). The statistical tests realized in Section 3.2 showed for these two rats no light-dark differences (p-values of 0.40 and 0.98 for light-dark differences, amplitude of the cosinor cannot be determined, no autocorrelation beyond the interval of confidence). Therefore, rats 1 and 4 were not included in further HR analysis.

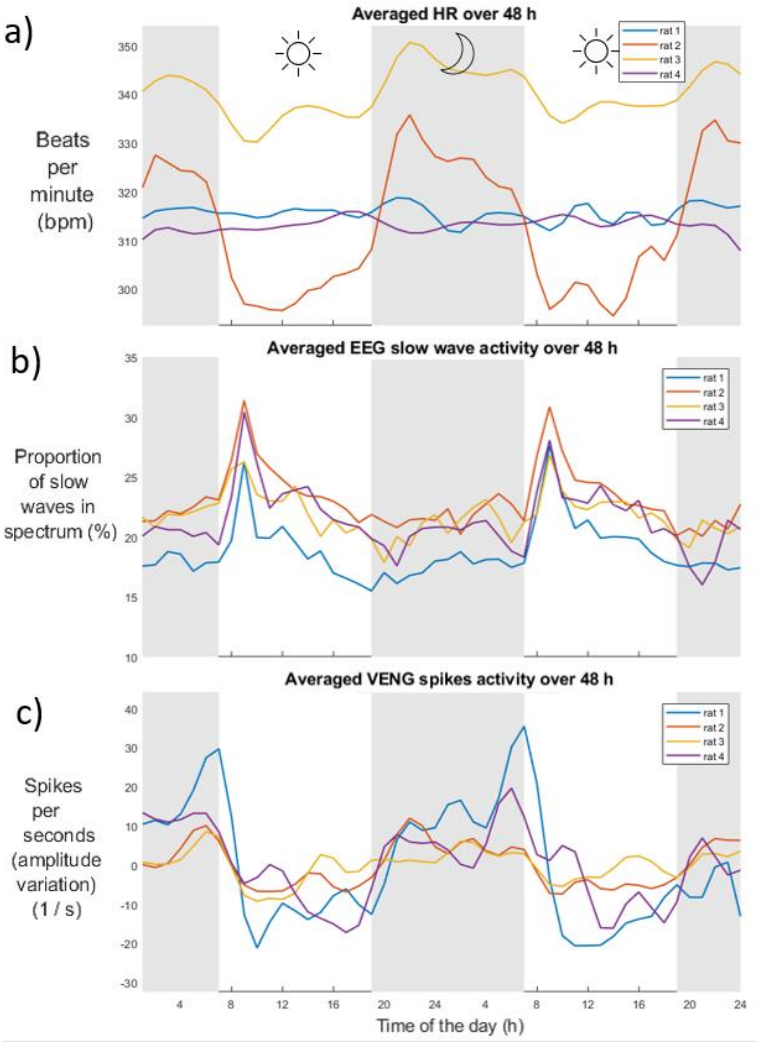

Figure 7. Inter animal comparison: a) HR rhythm b) EEG slow-wave activity c) VENG spike activity.

3.2. LIGHT-DARK VARIATIONS

In this section, statistical tests have been performed for all rats and for all physiological data (except the HR which has been discarded for rats 1 and 4). The duration of the recordings were 28 days for rats 1, 2, 4 and 21 days for rat 3. The physiological signals and statistical plots of rat 2 are detailed, as an illustration.

Cosine waves were fitted to each physiological data using a cosinor [30]. In all rats and all physiological signals, cosines show non-zero amplitude ($p < 0.01$) and a relatively high correlation (from 0.83 to 0.95 for HR, from 0.67 to 0.78 for EEG, from 0.61 to 0.81 for VENG spikes) with the corresponding metric. Figure 8 details, for rat 2, the same physiological signals (as in Figure 7), averaged of 48-hour samples, with corresponding standard deviation (relative to the averaging) and cosine fit (as shown in red). The same illustration is given for rats 1, 3 and 4, in supplementary materials, in Figures S1 to S3. Correlation between VENG and EEG is given, for rat 2, in supplementary materials, in Figure S10.

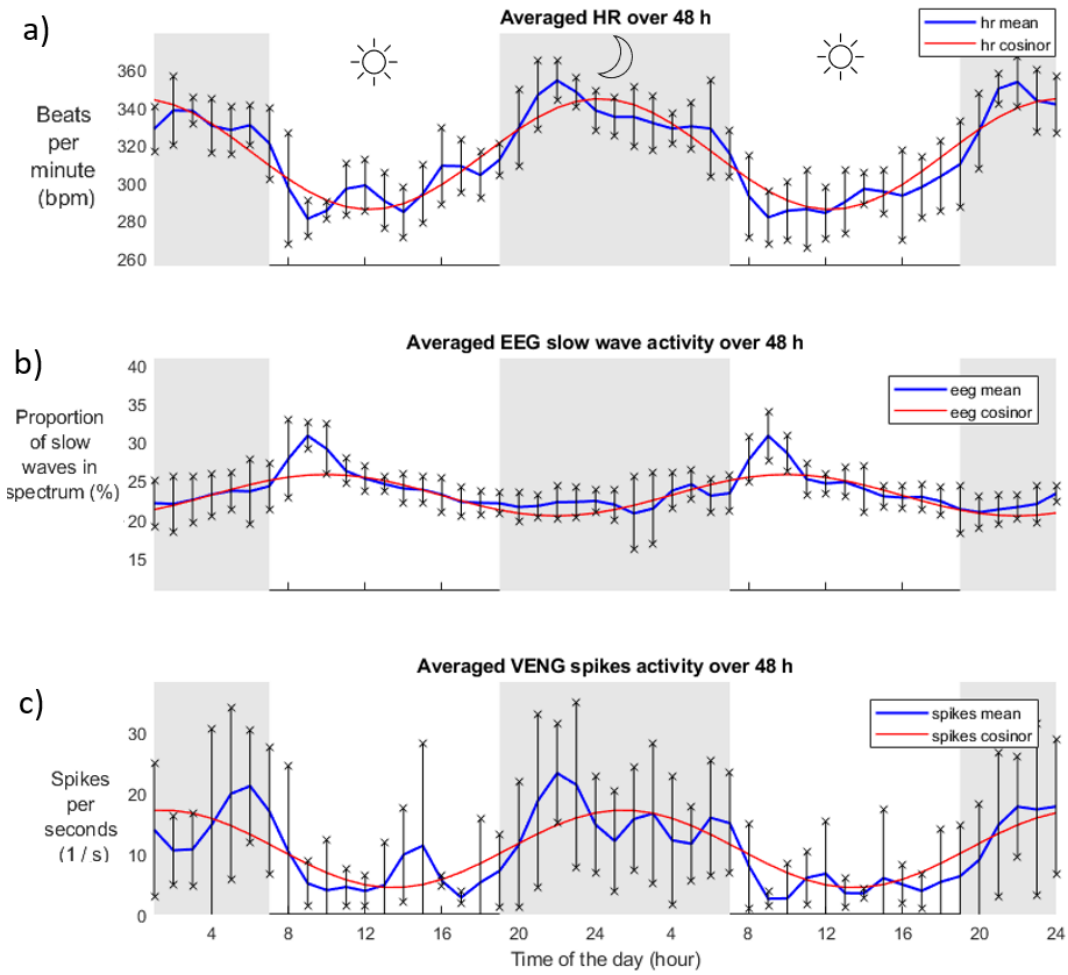

Figure 8. a) HR, b) EEG slow-wave activity and c) VENG spikes activity averaged on a one-hour time frame, and displayed over 48 hours, for rat 2. All values were averaged over the entire recording length (28 days). Data are plotted in blue (average) with gray bars (standard deviation). A cosinor fit is displayed in red. The light/dark periods are displayed in white/gray background.

We computed the spectral density, as estimated from the periodogram, for 5 and 10 days of recording. Figure 9 illustrates, for rat 2, the spectral density of HR, EEG slow-wave and VENG spike activities in a periodogram. The same illustration is given for rats 1, 3 and 4, in supplementary materials, in Figures S4 to S6. In all rats, the largest peak corresponds to 24h. The peak at 24 hours is significant for all physiological metrics, both with 5 and 10 days of recording (Fisher's g-statistic, $p < 0.01$). Other peaks are also visible on the figure, mainly related to harmonics of 24 hours, but this does not affect the significance of the main 24-hour peak. Also, the VENG peaks not corresponding to 24 hours are more prominent than the ones of HR and EEG slow waves, but are not significant in the periodogram.

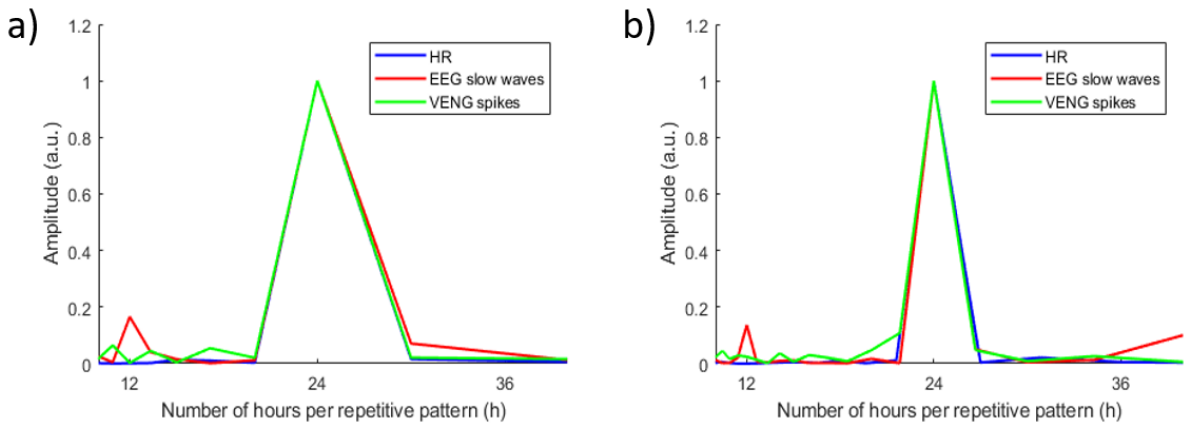

Figure 9. Periodograms of HR, EEG slow-wave and VENG spike activities, as obtained by Fourier analysis (with arbitrary units – normalized so that the spectrogram amplitude is equal to one for a 24-hour period) for rat 2. All metrics are averaged one-hour time frame. a) Over 5 days. b) Over 10 days.

We computed the autocorrelation of all metrics. For all rats, peaks corresponding to a period of 24 hours were seen, with values above 0.40 to 0.48, 0.35 to 0.48 and 0.35 to 0.43, respectively for HR, EEG slow-wave and VENG spike activities. Since these values exceed the confidence interval (see Methods), the 24-hour cycles are significant. Figure 10 illustrates, for rat 2, the autocorrelation function HR, EEG slow-wave and VENG spike activities, where peaks corresponding to a period of 24 hours can be clearly seen. The same illustration is given for rats 1, 3 and 4, in supplementary materials, in Figures S7 to S9.

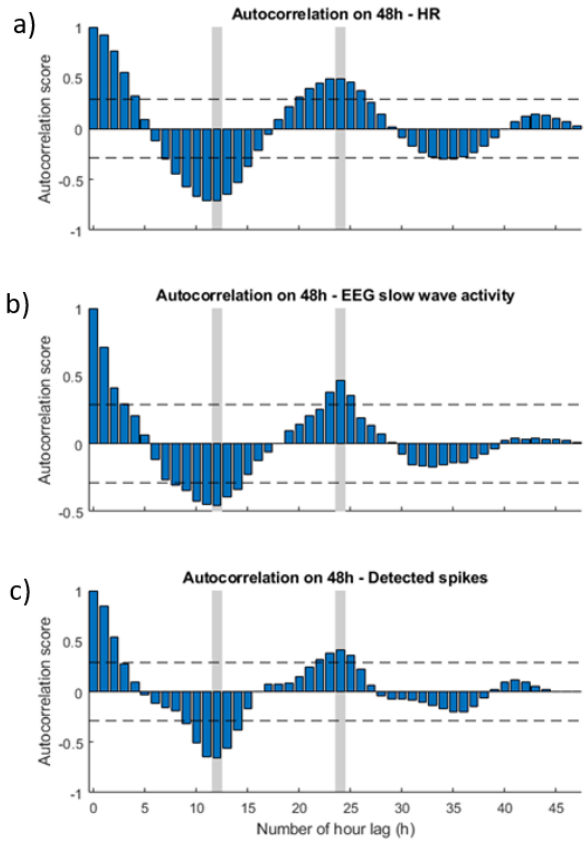

Figure 10. Autocorrelation of the averaged signal on a 48-hour basis for rat 2. The signal is correlated with itself, following a lag of 1 hour. The score of the resulting correlation is therefore dependent on the number of lags and can be displayed as a function. Autocorrelations of a) HR, b) EEG slow-wave activity and c) VENG spikes activity.

After checking that the means of the physiological signals were normally distributed, the data points were compared by one-way ANOVA tests: (1) between 2 consecutive periods of 24 h, (2) between the first and the second day, and (3) between the first night and the second night, to confirm the repeatability; and (4) between the first day and the first night to assess a light-dark cycle. For all rats, statistical tests (1), (2) and (3) showed no significant difference in mean values ($p > 0.2$), indicating that all physiological signals are consistent over two consecutive days. Statistical test (4) showed, for each physiological signal, a significant difference between the means on the first day and the first night ($p < 0.01$), thus demonstrating the light-dark cycle.

3.3. Recording Length

Since chronic animal experiments are demanding for the animal, time-consuming and costly, it is important to limit the duration of the experiment, and yet to reach a reasonable signal quality. In the two previous sections, the signal quality was significantly improved by averaging the 24-hour data samples over the entire recording time. It is expected that above a given duration, increasing the recording length will not significantly improve the signal quality. To clarify this point, the Pearson correlation coefficient of the average obtained with n days of signal extracted from the 28 days recording was calculated.

For the four rats, Figure 11 shows this correlation between the n first days average of each physiological signal (HR, EEG slow-wave and VENG spike activity) and the grand average (physiological signals averaged over the entire recording length). Averaging these correlations over the 4 rats, 2, 2 and 4 days are required to reach a very strong correlation of 80% with the grand average [37], for HR, EEG slow-wave and VENG spike activity respectively. Globally, about 7 days are required to reach a correlation above 90%, with small variations depending on the rat and physiological signal considered (see Figure 11).

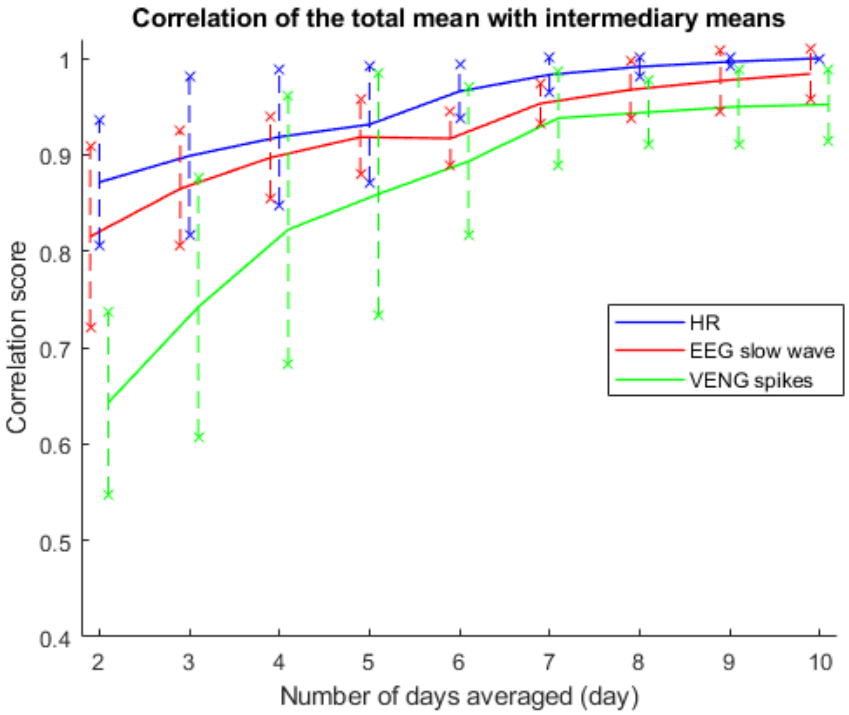

Figure 11. Correlation of each physiological signal (HR, EEG slow-wave and VENG spike activity) averaged over the n first days, with the grand average (physiological signals averaged over the entire recording length of 28 days).

4. DISCUSSION

4.1. MAJOR FINDINGS

Our results demonstrate that the light-dark cycles can be detected in long-term vagus nerve activity monitoring. The light-dark cycles derived from the spike activity analysis of the vagus nerve was compared with EEG slow waves recordings, which is an established signal for circadian studies. We also compared our results to HR estimation derived from the VENG recording. The periodogram, autocorrelation and cosinor fit highlighted the 24-hour repetitive pattern, and statistical tests confirmed significant differences between the dark and light periods for the EEG slow wave, HR and VENG spike activity. The recording length to characterize the light-dark cycles was also assessed. Investigating light-dark cycles based on VENG requires a recording period of about 7 days to reach a correlation above 90% with the averaged over the entire recording length.

4.2. CONTRIBUTION TO LIGHT-DARK CYCLES

This is the first study showing the light-dark cycles of the vagus nerve spike activity by direct means. We presented a methodological approach to chronically record directly continuous vagus nerve activities in rats. During preliminary trials, we were able to show for the first time the light-dark cycles of the vagus nerve spike activity. As a major outcome of this study, vagus nerve recordings hold the promise to help understand intricate functions such as the circadian regulation. The vagus nerve is indeed well known to be involved in respiratory regulation [32], BP, immune control [38], thermoregulation [39], and many other essential functions. In acute recordings, vagus nerve activity has been shown to correlate with physiological parameters such as respiration cycles [40] and baroreceptive fibers [41]. Since the vagus nerve activity is linked to physiological parameters driven by circadian modulations, it can be expected that the vagus nerve activity will exhibit a circadian pattern as well. This is also expected since the vagus nerve is a well-known major control pathway from the SCN to body functions [9].

Most previous studies on the connection between circadian rhythm and vagus nerve spike activity used indirect parameters and discontinuous sampling (e.g., blood samples and HR) [42]–[44]. For instance, a large study on humans reported the impact of the circadian system on cardiovascular function [42], where blood samples and physiological measurements were collected at regular intervals over a week. Those studies have shown circadian regulations in the vagal tone through heart-rate variability (HRV), quantifying the beat-to-beat interval variations. Besides, in rats, larger activities were previously found in dark periods compared to light periods, both in HR ([31], [45], [46]) and in BP ([47], [48]), which fits our findings in vagus nerve activity.

However, indirect measurements can show shortcomings. In particular, while vagal activity was believed to be correctly estimated by the HRV (i.e. through indirect measurement), direct vagus nerve monitoring showed that its activity was not correlated with HRV (with or without anesthesia) [49]. In this regard, direct and continuous measurements are expected to yield more information on different previously cited physiological parameters. For instance, the variations of HR and BP have been widely studied in rats using an implant recording the ECG [45], [46]. These studies could demonstrate the circadian rhythm of both parameters and the role of the autonomic nervous system. Hu *et al.* [31] also describe the circadian rhythm of the HR driven by the SCN thanks to an implant recording the ECG. By showing the circadian rhythm of the vagus nerve (by direct measurement), our results are in line with these previous findings evaluating vagal activity through ECG. The circadian rhythm has been studied

through direct continuous recording of BP, HR, EEG, but, except for Ogawa *et al.* [11], the vagus nerve activity has not been explored in that context.

While it has been possible to describe the circadian rhythm driven by the SCN through several means [50] and demonstrate the role of the vagus nerve in the circadian regulation through indirect means [9], [51], no circadian pattern was found in the vagus nerve activity in a previous study where the vagus nerve activity was recorded continuously [10]. Our results are non-concordant with those findings, but we believe the experimental conditions are different. Indeed, the main focus of [10] was to describe the neural activity related to congestive heart failure. Therefore, the focus was not on the role of the vagus nerve in circadian rhythm and the analysis was less sensitive in that regard. More specifically, although a circadian rhythm seems to be visible on their data, cosinor tests showed no significant circadian variation of vagal activity. This was evaluated on a signal that was high pass filtered, rectified, and summed over fixed time segments to represent the total nerve activity. We analyzed the vagus nerve activity through detected spikes, which is a more direct measurement of the nerve activity.

4.3. Potential application in epilepsy

The circadian rhythm has a strong impact on different types of pathology, such as epilepsy, a common neural disease. The rhythmicity of seizures has been known for years [52], [53], and recent advances in EEG monitoring have shown circadian seizure patterns in some patients [54]. Diurnal seizures cluster during certain times of the day, such as on awakening and late in the afternoon, whereas nocturnal seizures occur primarily at bedtime and in the hours before awakening [55], [56]. Seizures occur in patterns dependent on the pathophysiology of the epileptic condition [57], [58] and one hypothesis is that the circadian clock plays a crucial role in these. Circadian modulation varies with epilepsy syndrome and location of seizure foci. For example, frontal lobe seizures occur mostly during sleep with an early morning peak [59]. The role of the disruption of the circadian rhythm has also been demonstrated for sudden unexpected death in epilepsy (SUDEP) [60], the leading cause of epilepsy-related death in patients with refractory epilepsy. Convergent lines of evidence suggest that SUDEP occurs due to seizure-induced perturbation of respiratory, cardiac, and cerebral function as well as other potential predisposing factors [61]. It is consistently observed that SUDEP happens more during the night and the early hours of the morning. In addition, seizure-related laryngospasm may induce obstructive apnea leading to ventricular fibrillation and a cause for SUDEP [62]. Since the vagus nerve exhibits circadian regulations as demonstrated by our results and is affected by seizures [16], [17], it may be important to take both forms of modulation into account. Besides, since the vagus nerve is connected to the larynx and the laryngospasm could potentially be recorded, the monitoring of the vagus nerve activity could also help in the understanding of potential causes of SUDEP [62] since the laryngospasm could potentially be recorded.

In addition, this study is of specific interest for further research in the field of epilepsy because vagus nerve stimulation (VNS) is being used as an additional treatment for refractory epilepsy. It has been previously shown that an on-demand VNS has a beneficial effect on seizure reduction [63], [64]. Current on-demand stimulations are triggered by a magnet, activated by the patient or an automated algorithm based on the detection of ictal tachycardia [63], [65]. However, all the patients may not experience tachycardia [66]. Stumpp *et al.* [17] proposed a seizure detection algorithm based on vagus nerve activity during acute recordings. Therefore, vagus nerve activity could be used as the trigger for on-demand stimulation, enabling the possibility to stimulate the vagus nerve based on the activity recorded from the stimulating electrodes. In this study, the light-dark cycle has been found to impact VENG and therefore, in a chronic setting, it is likely that the VENG seizure detection threshold should

be adapted to these variations. For example, the method used by Stumpp *et al.* [17] is adaptive and could potentially manage the light-dark cycle variability.

4.4. LIMITATIONS AND FURTHER WORKS

We observed VENG spike activity increase at nighttime. It may be surprising, as rats are nocturnal. Therefore, during daytime, when the rats are less active, there is a decrease in HR, hence we could expect to record increased vagus nerve activity. However, we believe that the meaning of this result should be taken with precautions. The vagus nerve also contains many fibers that are unrelated to cardiac activity [67]. Indeed, the largest contingent of fibers is afferent, and it might appear logical that afferent neural activity is reduced when animals are at rest. Unfortunately, we do not know exactly from what type of fibers the signals are being recorded. Only part of the vagus nerve activity is recorded, potentially accounting for only some of the vagus nerve functions. The expectation is that large myelinated fibers contribute the most but thin fibers are more numerous.

The HR was extracted from the processed VENG (see Methods) and yields similar results compared to the ones found in [31] (315 ± 16 bpm in our work, versus 341 ± 20 bpm in [31]), which supports the validity of our HR estimation method. The Bland-Altman plot comparing our VENG-based HR with HR derived from ECG (see Figure 4) showed that our method is associated with a normal error distribution which decreases when considering a longer period of estimation, with a standard deviation of 6 bpm for a 10-min window. In the context of chronic implants, this method does not require ECG electrodes, therefore it enables reducing the number of electrodes at different recording sites and the number of amplifiers needed. Reduced implant size and lower electronic failure rates are obvious benefits, in addition to fewer interference if using an implanted wireless ECG [15]. Our HR extraction method does not enable a precise beat-to-beat HR estimation and hence neither an estimation of the HRV, commonly reported in medical studies. Also, one should note that the preliminary experimentation was realized in rats under ketamine anesthesia, to record easily simultaneously ECG, and therefore be able to validate the method. This situation differs from freely moving rats, and explains, for instance, the variation in HR due to anesthesia: there is a slower HR in freely moving rats (e.g. 315 ± 16 bpm in our work or 341 ± 20 bpm in [31]), and faster one in rats under ketamine anesthesia (e.g. 445 ± 21 bpm in our work or 432 ± 11 bpm in [29]). Movement artifacts could also play a role in awake rats. However, we believe it was mitigated since only portions of the signal without motion artifact were kept.

Only two of our four rats showed the characteristic light-dark cycles in HR. We believe it is a limitation of our method since HR circadian rhythm was expected in all rats. Indeed, a circadian rhythm is present in the HR in rats [68], [69] and mice [69]. Besides, in all rats (and therefore including the two not showing HR light-dark cycles), light-dark cycles were found for EEG and VENG activity. We found no clear reason for this shortcoming, this is potentially linked to the data processing. For instance, the positive trend seen in the Bland-Altman plot (Figure 4) could explain a reduction of 2.5 bpm in a 30-bpm full amplitude variation. This alone cannot explain the absence of clear light-dark cycles circadian changes in HR response in two of our four rats. Specific care was taken to ensure that the rats were not stressed. Yet, it cannot be stated that the physiology of the rats was not disturbed. Further research is needed, and a comparison with HR obtained through ECG will help to determine the validity of the HR estimation method in various situations. This goes beyond the work presented in this study. However, despite this limitation, we think that this method deserves to be reported because of its potential benefits, specifically in a chronic setting (see previous paragraph), and we acknowledge the current limitations.

In this study, the VENG recordings were validated through: a preliminary acute experiment, electrodes impedances control, spike detection and analysis, and post-mortem dissection. Whilst large variations

in impedance are suggestive of adverse reactions and poor implant response, measuring impedances within an expected range does not guarantee functional implants [46]. Physiological responses to electrical stimuli should be included for further validation.

Although a limited number of animals were used in this pilot study, our results demonstrate the feasibility of light-dark cycle modulation analysis in VENG recording. We included only males to not be confronted to eventual gender differences. Larger numbers of rats will be necessary to investigate further the circadian rhythm in vagus nerve activity, to evaluate gender related differences, or quantify differences between healthy and pathological conditions, for instance.

Further studies should also investigate afferent and efferent activities in the VENG. The current setup uses a three-electrode cuff, and therefore one could analyze the differential voltages between the first two and last two electrodes separately. By analyzing these two differential signals separately, afferent and efferent activities could perhaps be distinguished on the basis of time delay. However, a small interelectrode distance will result in spatial aliasing, i.e., poor spatial differentiation in the recorded signal due to a fast action potential velocity compared to the small recording interelectrode distance. As previously mentioned [28], with the current setup, spatial aliasing will occur for fibers larger than 3 µm. Therefore, a subset of the spectrum of fiber diameters nerve could be analyzed in the rat vagus with the current setup. For further studies, the setup could be adapted to address this. More specifically, in order to fully distinguish all afferent and efferent activities of the vagus nerve fibers, larger inter-electrode distance or specific electrodes (e.g., [12], [15]) could be considered.

In this work, we record globally spontaneous firing without distinguishing among fiber types. Moreover, the extra neural recording used is prone to capture only large, myelinated fibers, and the content of thick myelinated fibers may vary between species. Therefore, the extractability to humans remains to be determined. Nevertheless, the vagus nerve carries various common physiological functions between animals and humans. Therefore, we may suspect similar day-night variations of vagus nerve activity in humans, although the temporal presentation differs. Indeed, rats are typically more active at night, while humans are not. Future device development capable of recording spontaneous vagus nerve activity in humans will hopefully be able to answer these questions.

In addition, to further elucidate the complexity of the vagus nerve activity and circadian rhythm, VENG could be compared to additional physiological measures, also known to be impacted by the circadian rhythm, such as temperature, motion, respiration and HR variation.

5. CONCLUSION

In conclusion, we have demonstrated how light-dark cycles can be detected in long-term vagus nerve activity monitoring. We provide a direct measurement of the circadian regulations in the vagus nerve activity. We also investigated the recording length required to characterize accurately light-dark cycles, and found that 7 days are sufficient to reach a correlation above 90%. This research opens the doors to other investigations, for instance in the context of epilepsy.

6. ACKNOWLEDGEMENT

This work has been funded by the Pôle Mecatech of the Walloon Region (Belgium) and by the fund Van Buuren-Jaumotte-Demoulin. We are grateful for the help provided by Geoffrey Vanbienne in the realisation of our hardware setup.

7. REFERENCES

[1] R. M. Buijs and A. Kalsbeek, "Hypothalamic integration of central and peripheral clocks," *Nature Reviews Neuroscience*, vol. 2, no. 7, pp. 521–526, 2001, doi: 10.1038/35081582.

[2] H. Terazono *et al.*, "Adrenergic regulation of clock gene expression in mouse liver," *Proc Natl Acad Sci U S A*, vol. 100, no. 11, pp. 6795–6800, 2003, doi: 10.1073/pnas.0936797100.

[3] M. Astiz, I. Heyde, and H. Oster, "Mechanisms of communication in the Mammalian Circadian timing system," *International Journal of Molecular Sciences*, vol. 20, no. 2, 2019, doi: 10.3390/ijms20020343.

[4] M. Makino, H. Hayashi, H. Takezawa, M. Hirai, H. Saito, and S. Ebihara, "Circadian rhythms of cardiovascular functions are modulated by the baroreflex and the autonomic nervous system in the rat," *Circulation*, vol. 96, no. 5, pp. 1667–1674, 1997, doi: 10.1161/01.CIR.96.5.1667.

[5] J. Oosting, H. A. J. Struijker-Boudier, and B. J. A. Janssen, "Autonomic control of ultradian and circadian rhythms of blood pressure, heart rate, and baroreflex sensitivity in spontaneously hypertensive rats," *Journal of Hypertension*, vol. 15, no. 4, pp. 401–410, 1997, doi: 10.1097/00004872-199715040-00011.

[6] K. Hu, F. A. J. L. Scheer, R. M. Buijs, and S. A. Shea, "The circadian pacemaker generates similar circadian rhythms in the fractal structure of heart rate in humans and rats," *Cardiovascular Research*, vol. 80, no. 1, pp. 62–68, 2008, doi: 10.1093/cvr/cvn150.

[7] F. A. J. L. Scheer *et al.*, "Impact of the human circadian system, exercise, and their interaction on cardiovascular function," *Proc Natl Acad Sci U S A*, vol. 107, no. 47, pp. 20541–20546, 2010, doi: 10.1073/pnas.1006749107.

[8] N. Black *et al.*, "Circadian rhythm of cardiac electrophysiology, arrhythmogenesis, and the underlying mechanisms," *Heart Rhythm*, vol. 16, no. 2, pp. 298–307, 2019, doi: 10.1016/j.hrthm.2018.08.026.

[9] H. Bando, T. Nishio, G. T. J. Van Der Horst, S. Masubuchi, Y. Hisa, and H. Okamura, "Vagal regulation of respiratory clocks in mice," *Journal of Neuroscience*, vol. 27, no. 16, pp. 4359–4365, 2007, doi: 10.1523/JNEUROSCI.4131-06.2007.

[10] M. Ogawa *et al.*, "Left Stellate Ganglion and Vagal Nerve Activity and Cardiac Arrhythmias in Ambulatory Dogs With Pacing-Induced Congestive Heart Failure," *J Am Coll Cardiol*, vol. 50, no. 4, pp. 335–343, 2007, doi: 10.1016/j.jacc.2007.03.045.

[11] M. Ogawa *et al.*, "Left Stellate Ganglion and Vagal Nerve Activity and Cardiac Arrhythmias in Ambulatory Dogs With Pacing-Induced Congestive Heart Failure," *J Am Coll Cardiol*, vol. 50, no. 4, pp. 335–343, 2007, doi: 10.1016/j.jacc.2007.03.045.

[12] J. D. Falcone *et al.*, "A novel microwire interface for small diameter peripheral nerves in a chronic, awake murine model," *J Neural Eng*, vol. 17, no. 4, p. 046003, 2020, doi: 10.1088/1741-2552/ab9b6d.

[13] G. A. McCallum *et al.*, "Chronic neural activity recorded within breast tumors," *Scientific Reports*, vol. 10, no. 1, pp. 1–13, 2020, doi: 10.1038/s41598-020-71670-y.

[14] G. A. McCallum *et al.*, “Chronic interfacing with the autonomic nervous system using carbon nanotube (CNT) yarn electrodes,” *Scientific Reports*, vol. 7, no. 1, pp. 1–14, 2017, doi: 10.1038/s41598-017-10639-w.

[15] J. T. Marmerstein, G. A. McCallum, and D. M. Durand, “Direct measurement of vagal tone in rats does not show correlation to HRV,” *Scientific Reports*, vol. 11, no. 1, pp. 1–12, 2021, doi: 10.1038/s41598-020-79808-8.

[16] L. Stumpp *et al.*, “Recording of spontaneous vagus nerve activity during Pentylenetetrazol-induced seizures in rats,” *Journal of Neuroscience Methods*, vol. 343, p. 108832, Sep. 2020, doi: 10.1016/j.jneumeth.2020.108832.

[17] L. Stumpp *et al.*, “Vagus Nerve Electroneurogram-Based Detection of Acute Pentylenetetrazol Induced Seizures in Rats,” *International Journal of Neural Systems*, vol. 31, no. 7, pp. 1–17, 2021, doi: 10.1142/S0129065721500246.

[18] P. Sabetian, M. R. Popovic, and P. B. Yoo, “Optimizing the design of bipolar nerve cuff electrodes for improved recording of peripheral nerve activity,” *J Neural Eng*, vol. 14, no. 3, Mar. 2017, doi: 10.1088/1741-2552/AA6407.

[19] H. Smets *et al.*, “Journal of Neural Engineering Analysing vagus nerve spontaneous activity using finite element modelling,” *Journal of Neural Engineering*, vol. 18, no. 5, p. 56008, 2021, doi: 10.1088/1741-2552/abe68f.

[20] Y. Medlej *et al.*, “Enhanced setup for wired continuous long-term EEG monitoring in juvenile and adult rats: application for epilepsy and other disorders,” *BMC Neuroscience*, vol. 20, no. 1, pp. 1–12, 2019, doi: 10.1186/s12868-019-0490-z.

[21] A. Nonclercq and P. Mathys, “Reduction of power line interference using active electrodes and a driven-right-leg circuit in electroencephalographic recording with a minimum number of electrodes,” in *Annual International Conference of the IEEE Engineering in Medicine and Biology - Proceedings*, 2004, vol. 26 III.

[22] A. Nonclercq and P. Mathys, “Quantification of motion artifact rejection due to active electrodes and driven-right-leg circuit in spike detection algorithms,” *IEEE Transactions on Biomedical Engineering*, vol. 57, no. 11, pp. 2746–2752, 2010, doi: 10.1109/TBME.2010.2055867.

[23] H. Smets *et al.*, “Analysing vagus nerve spontaneous activity using finite element modelling,” *Journal of Neural Engineering*, vol. 18, no. 5, p. 56008, 2021, doi: 10.1088/1741-2552/abe68f.

[24] L. Stumpp *et al.*, “Vagus Nerve Electroneurogram-Based Detection of Acute Pentylenetetrazol Induced Seizures in Rats,” *International Journal of Neural Systems*, vol. 31, no. 7, pp. 1–17, 2021, doi: 10.1142/S0129065721500246.

[25] H. P. Landolt, D. J. Dijk, P. Achermann, and A. A. Borbély, “Effect of age on the sleep EEG: Slow-wave activity and spindle frequency activity in young and middle-aged men,” *Brain Research*, vol. 738, no. 2, pp. 205–212, 1996, doi: 10.1016/S0006-8993(96)00770-6.

[26] A. Nonclercq *et al.*, “Spike detection algorithm automatically adapted to individual patients applied to spike and wave percentage quantification,” *Neurophysiologie Clinique*, vol. 39, no. 2, 2009, doi: 10.1016/j.neucli.2008.12.001.

[27] A. Nonclercq *et al.*, “Cluster-based spike detection algorithm adapts to interpatient and intrapatient variation in spike morphology,” *Journal of Neuroscience Methods*, vol. 210, no. 2, pp. 259–265, 2012, doi: 10.1016/j.jneumeth.2012.07.015.

[28] H. Smets *et al.*, “Analysing vagus nerve spontaneous activity using finite element modelling,” *Journal of Neural Engineering*, vol. 18, no. 5, p. 56008, 2021, doi: 10.1088/1741-2552/abe68f.

[29] M. O. Carruba, G. Pietro Bondiolotti, G. B. Picotti, N. Catteruccia, and M. Da Prada, “Effects of diethyl ether, halothane, ketamine and urethane on sympathetic activity in the rat,” *European Journal of Pharmacology*, vol. 134, no. 1, pp. 15–24, 1987, doi: 10.1016/0014-2999(87)90126-9.

[30] R. Refinetti, G. Cornélissen, and F. Halberg, *Procedures for numerical analysis of circadian rhythms*, vol. 38, no. 4. 2007. doi: 10.1080/09291010600903692.

[31] K. Hu, F. A. J. L. Scheer, R. M. Buijs, and S. A. Shea, “The circadian pacemaker generates similar circadian rhythms in the fractal structure of heart rate in humans and rats,” *Cardiovascular Research*, vol. 80, no. 1, pp. 62–68, 2008, doi: 10.1093/cvr/cvn150.

[32] H. Bando, T. Nishio, G. T. J. Van Der Horst, S. Masubuchi, Y. Hisa, and H. Okamura, “Vagal regulation of respiratory clocks in mice,” *Journal of Neuroscience*, vol. 27, no. 16, pp. 4359–4365, 2007, doi: 10.1523/JNEUROSCI.4131-06.2007.

[33] R. Refinetti, G. Cornélissen, and F. Halberg, *Procedures for numerical analysis of circadian rhythms*, vol. 38, no. 4. 2007. doi: 10.1080/09291010600903692.

[34] G. Cornelissen, “Cosinor-based rhythmometry,” *Theoretical Biology and Medical Modelling*, vol. 11, no. 1. BioMed Central Ltd., Apr. 11, 2014. doi: 10.1186/1742-4682-11-16.

[35] H. Akoglu, “User’s guide to correlation coefficients,” *Turkish Journal of Emergency Medicine*, vol. 18, no. 3, pp. 91–93, 2018, doi: 10.1016/j.tjem.2018.08.001.

[36] R. Refinetti, G. Cornélissen, and F. Halberg, *Procedures for numerical analysis of circadian rhythms*, vol. 38, no. 4. 2007. doi: 10.1080/09291010600903692.

[37] H. Akoglu, “User’s guide to correlation coefficients,” *Turkish Journal of Emergency Medicine*, vol. 18, no. 3, pp. 91–93, 2018, doi: 10.1016/j.tjem.2018.08.001.

[38] M. N. Jarczok, H. Guendel, J. J. McGrath, and E. M. Balint, “Circadian Rhythms of the Autonomic Nervous System: Scientific Implication and Practical Implementation,” *Chronobiology - The Science of Biological Time Structure*, pp. 1–20, 2019, doi: 10.5772/intechopen.86822.

[39] M. Székely, “The vagus nerve in thermoregulation and energy metabolism,” *Autonomic Neuroscience: Basic and Clinical*, vol. 85, no. 1–3, pp. 26–38, 2000, doi: 10.1016/S1566-0702(00)00217-4.

[40] C. Sevcencu and J. J. Struijk, “Autonomic alterations and cardiac changes in epilepsy,” *Epilepsia*, vol. 51, no. 5. Epilepsia, pp. 725–737, May 2010. doi: 10.1111/j.1528-1167.2009.02479.x.

[41] J. Rozman and S. Ribarič, “Selective recording of electroneurograms from the left vagus nerve of a dog during stimulation of cardiovascular or respiratory systems,” *Chinese Journal of Physiology*, vol. 50, no. 5, pp. 240–250, 2007.

[42] F. A. J. L. Scheer *et al.*, “Impact of the human circadian system, exercise, and their interaction on cardiovascular function,” *Proc Natl Acad Sci U S A*, vol. 107, no. 47, pp. 20541–20546, 2010, doi: 10.1073/pnas.1006749107.

[43] J. F. J. Morrison and S. B. Pearson, “The effect of the circadian rhythm of vagal activity on bronchomotor tone in asthma,” *British Journal of Clinical Pharmacology*, 1989.

[44] P. Boudreau, W. H. Yeh, G. A. Dumont, and D. B. Boivin, “A circadian rhythm in heart rate variability contributes to the increased cardiac sympathovagal response to awakening in the morning,” *Chronobiology International*, vol. 29, no. 6, pp. 757–768, 2012, doi: 10.3109/07420528.2012.674592.

[45] M. Makino, H. Hayashi, H. Takezawa, M. Hirai, H. Saito, and S. Ebihara, “Circadian rhythms of cardiovascular functions are modulated by the baroreflex and the autonomic nervous system in the rat,” *Circulation*, vol. 96, no. 5, pp. 1667–1674, 1997, doi: 10.1161/01.CIR.96.5.1667.

[46] J. Oosting, H. A. J. Struijker-Boudier, and B. J. A. Janssen, “Autonomic control of ultradian and circadian rhythms of blood pressure, heart rate, and baroreflex sensitivity in spontaneously hypertensive rats,” *Journal of Hypertension*, vol. 15, no. 4, pp. 401–410, 1997, doi: 10.1097/00004872-199715040-00011.

[47] M. Makino, H. Hayashi, H. Takezawa, M. Hirai, H. Saito, and S. Ebihara, “Circadian rhythms of cardiovascular functions are modulated by the baroreflex and the autonomic nervous system in the rat,” *Circulation*, vol. 96, no. 5, pp. 1667–1674, 1997, doi: 10.1161/01.CIR.96.5.1667.

[48] J. Oosting, H. A. J. Struijker-Boudier, and B. J. A. Janssen, “Autonomic control of ultradian and circadian rhythms of blood pressure, heart rate, and baroreflex sensitivity in spontaneously hypertensive rats,” *Journal of Hypertension*, vol. 15, no. 4, pp. 401–410, 1997, doi: 10.1097/00004872-199715040-00011.

[49] J. T. Marmerstein, G. A. McCallum, and D. M. Durand, “Direct measurement of vagal tone in rats does not show correlation to HRV,” *Scientific Reports*, vol. 11, no. 1, pp. 1–12, 2021, doi: 10.1038/s41598-020-79808-8.

[50] N. Black *et al.*, “Circadian rhythm of cardiac electrophysiology, arrhythmogenesis, and the underlying mechanisms,” *Heart Rhythm*, vol. 16, no. 2, pp. 298–307, 2019, doi: 10.1016/j.hrthm.2018.08.026.

[51] F. A. J. L. Scheer *et al.*, “Impact of the human circadian system, exercise, and their interaction on cardiovascular function,” *Proc Natl Acad Sci U S A*, vol. 107, no. 47, pp. 20541–20546, 2010, doi: 10.1073/pnas.1006749107.

[52] W. Ae. Hofstra and A. W. de Weerd, “The circadian rhythm and its interaction with human epilepsy: A review of literature,” *Sleep Medicine Reviews*, vol. 13, no. 6, pp. 413–420, 2009, doi: 10.1016/j.smrv.2009.01.002.

[53] M. Quigg, “Circadian rhythms: Interactions with seizures and epilepsy,” *Epilepsy Research*, vol. 42, no. 1, pp. 43–55, 2000, doi: 10.1016/S0920-1211(00)00157-1.

[54] S. Khan *et al.*, “Circadian rhythm and epilepsy,” *The Lancet Neurology*, vol. 17, no. 12, pp. 1098–1108, 2018, doi: 10.1016/S1474-4422(18)30335-1.

[55] M. Langdon-Down and W. R. Brain, “Time of day in relation to convulsions in epilepsy,” *The Lancet*, 1929.

[56] G. Griffiths and J. T. Fox, “Rhythm in epilepsy,” *The Lancet*, 1938.

[57] M. Quigg, M. Straume, M. Menaker, and E. H. Bertram, “Temporal distribution of partial seizures: Comparison of an animal model with human partial epilepsy,” *Annals of Neurology*, vol. 43, no. 6, pp. 748–755, 1998, doi: 10.1002/ana.410430609.

[58] E. Taubøll, A. Lundervold, and L. Gjerstad, “Temporal distribution of seizures in epilepsy,” *Epilepsy Research*, vol. 8, no. 2, pp. 153–165, 1991, doi: 10.1016/0920-1211(91)90084-S.

[59] C. P. Derry and S. Duncan, “Sleep and epilepsy,” *Epilepsy and Behavior*, vol. 26, no. 3, pp. 394–404, 2013, doi: 10.1016/j.yebeh.2012.10.033.

[60] H. Persson, E. Kumlien, M. Ericson, and T. Tomson, “Circadian variation in heart-rate variability in localization-related epilepsy,” *Epilepsia*, vol. 48, no. 5, pp. 917–922, 2007, doi: 10.1111/j.1528-1167.2006.00961.x.

[61] H. Persson, E. Kumlien, M. Ericson, and T. Tomson, “Circadian variation in heart-rate variability in localization-related epilepsy,” *Epilepsia*, vol. 48, no. 5, pp. 917–922, 2007, doi: 10.1111/j.1528-1167.2006.00961.x.

[62] M. Stewart, “An explanation for sudden death in epilepsy (SUDEP),” *Journal of Physiological Sciences*, vol. 68, no. 4, pp. 307–320, 2018, doi: 10.1007/s12576-018-0602-z.

[63] P. Boon *et al.*, “Programmed and magnet-induced vagus nerve stimulation for refractory epilepsy,” *Journal of Clinical Neurophysiology*, vol. 18, no. 5. Lippincott Williams and Wilkins, pp. 402–407, 2001. doi: 10.1097/00004691-200109000-00003.

[64] R. S. Fisher and A. L. Velasco, “Electrical brain stimulation for epilepsy,” *Nature Reviews Neurology*, vol. 10, no. 5, pp. 261–270, 2014, doi: 10.1038/nrneurol.2014.59.

[65] R. S. Fisher and A. L. Velasco, “Electrical brain stimulation for epilepsy,” *Nature Reviews Neurology*, vol. 10, no. 5, pp. 261–270, 2014, doi: 10.1038/nrneurol.2014.59.

[66] P. Boon *et al.*, “A prospective, multicenter study of cardiac-based seizure detection to activate vagus nerve stimulation,” *Seizure*, vol. 32, pp. 52–61, 2015, doi: 10.1016/j.seizure.2015.08.011.

[67] J. A. Clancy, S. A. Deuchars, and J. Deuchars, “The wonders of the Wanderer,” *Experimental Physiology*, vol. 98, no. 1, pp. 38–45, 2013, doi: 10.1113/expphysiol.2012.064543.

[68] K. Hu, F. A. J. L. Scheer, R. M. Buijs, and S. A. Shea, “The circadian pacemaker generates similar circadian rhythms in the fractal structure of heart rate in humans and rats,” *Cardiovascular Research*, vol. 80, no. 1, pp. 62–68, 2008, doi: 10.1093/cvr/cvn150.

[69] N. Black *et al.*, “Circadian rhythm of cardiac electrophysiology, arrhythmogenesis, and the underlying mechanisms,” *Heart Rhythm*, vol. 16, no. 2, pp. 298–307, 2019, doi: 10.1016/j.hrthm.2018.08.026.